14

Multivariate Differencing Techniques for Land Cover Change Detection: the Normalized Difference Reflectance Approach

Paolo Villa*, Giovanmaria Lechi** and Mario A. Gomarasca*
** Institute for Electromagnetic Sensing of the Environment (CNR-IREA), National Research Council, Milan, Italy*
*** Bulding Environment Sciences and Technology (BEST) Department, Polytechnic of Milan, Italy*

1. Introduction

The importance of the dynamic side of natural and man-made phenomena has become an urgent need when trying to mitigate the human impact on environment. Remote Sensing is one of the most effective way to quantify and map the changes of environmental conditions on our planet: the tools used for this purpose are called Change Detection Techniques. Techniques among which an important role is played by those methodologies based on multi-spectral remote sensing data and exploiting multivariate analysis derived methodologies, also demonstrating their capabilities through some test cases, covering flood events and urban growth studies.

Multi-temporal and multi-spectral techniques for Change Detection exist in a wide variety of approaches, often far too sector oriented and not straightforward. Compression and decorrelation techniques, on the other side, tend not to exploit the whole spectral content of remotely sensed data. The Normalized Difference Reflectance (NDR) here introduced is a general approach for bi-temporal land cover change mapping and detection that exploits the whole spectral capabilities of panchromatic, multi-spectral or hyper-spectral images. NDR is a general and simple measure that can be used in the frame of what are called Normalized Difference Change Detection Techniques (NDCD), which starts using as a input the NDR derived results. This Chapter includes a large test case which is a good benchmark for NDR approach, using Minimum Noise Fraction implementation of NDCD for mapping Hurricane Katrina aftermaths over the city of New Orleans, U.S., thus fusing together urban and flood change applications.

The purpose of the chapter is to give an overview of multivariate difference-based techniques for land cover change mapping using multispectral remote sensing data, and to introduce and demonstrate the Normalized Difference Reflectance approach in the frame of Normalized Difference Change Detection techniques. Two examples of NDCD results are given as a complement to theoretical aspects of the methodology, and an application study has been used as benchmark for the technique performances evaluation, in comparison with other established Change Detection techniques.

2. Multivariate Differences in Change Detection

Multi-temporal differencing is an established change detection technique for environmental mapping and monitoring with remotely sensed data (Singh, 1989; Lu et al., 2004; Coppin et al., 2004). Following a difference normalization approach, introduced in remote sensing for vegetation studies with the normalized difference vegetation index (NDVI), a multi-temporal implementation of this standardization technique for forest change analysis was first proposed for univariate vegetation indexes (VIs) (Coppin & Bauer, 1994), and then in comparison with other change detection methodologies (Coppin et al., 2001), always for forest mapping purposes.

During this work it has been introduced a quantitative method to evaluate land cover change through multi-spectral variation in radiometric response of surface features. In order to detect interesting changes, a pair of satellite scenes, geometrically registered and atmospherically corrected, is to be radiometrically normalized. After that, a map of spectral variations is produced using a multi-spectral difference index named Normalized Difference Reflectance (NDR). The NDR is therefore an approach to Change Feature Identification phase in Change Detection.

The phase of Change Mapping is then performed using NDR measures as inputs for Change Detection methodologies and techniques, in the frame of what are called Normalized Difference Change Detection (NDCD) techniques. The NDCD is a technique which, given an image pair, performs calculations on radiometric normalized reflectance data through the definition of the normalized difference reflectance (NDR) and produces a standardized difference of the reflectance values.

The use of NDR and NDCD will be presented through case studies showing change analysis covering flood events and urban environment: one case is over a flood event occurred in Bangladesh and exploiting Landsat-7/ETM+ scenes, another case regards the urban expansion scenario of Washington outskirts, U.S., and exploiting Terra ASTER data, the last and most complete case study is the analysis of the damages to the urban area of the city of New Orleans (Louisiana, USA) resulting from the passage of hurricane Katrina, using both SPOT-4/HRVIR and Landsat-5/TM data.

3. Normalized Difference Reflectance (NDR)

The Normalized Difference Reflectance (NDR) here introduced is a general approach for bi-temporal land cover change mapping and detection that exploits the whole spectral capabilities of panchromatic, multi-spectral or hyper-spectral images. Given an image pair, the NDR produces a standardized difference by analyzing the changes in the reflectance properties of each spectral band, so without losing any spectral richness as when applying indexes, feature reduction or compression techniques (Villa & Lechi, 2007).

The image reflectance differences were modified to a normalized version on the sum of spectral values, in order to minimize the confusion among difference values which are numerically equal, but come from different land cover change events.

Hence, for every spectral band the NDR is defined as follows:

$$NDR_j = \frac{R_j^{norm}(post) - R_j^{norm}(pre)}{R_j^{norm}(post) + R_j^{norm}(pre)} \quad (1)$$

where:
NDR = normalized difference reflectance
R^{norm} (post) = normalized reflectance for the post flood scene
R^{norm} (pre) = normalized reflectance for the pre flood scene
j = spectral band number

The NDR is a multi-spectral quantity which spans over the range of values from -1 to +1 and shows the amount of change in surface reflectance for every band in the original data, in terms of the relative difference in spectral signature of ground objects (-1.00 = maximum reflectance decrease, 0.00 = no change, +1.00= maximum reflectance increase). This approach is a quantitative base for building the successive phase of change detection, through the use of multi-spectral normalized reflectance values. A first and simple visual inspection of NDR band compositions permits a prompt and clear preliminary assessment of changes, thus supporting the choice of an apt change detection algorithm or technique for the phase of change mapping. Figure 1 shows an example of NDR calculated for calculated for an urban scenario, located in Maryland, U.S, using multi-temporal Terra ASTER data.

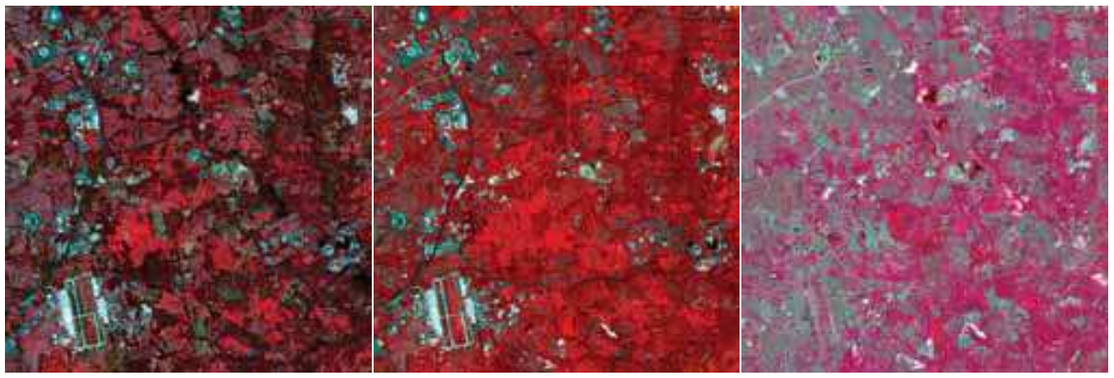

a) **b)** **c)**

Fig. 1. NDR calculated for an urban scenario, located in Maryland, U.S.: CIR visualization (RGB=3N,2,1), ASTER scene of April 9th, 2000 (a); CIR visualization (RGB=3N,2,1), ASTER scene of August 24th, 2003 (b); CIR visualization (RGB=3N,2,1), NDR values derived (c). Different colours in (c) are inked to different kind of variations in surface reflectance between (a) and (b) images: grey areas represent not changed features, cyan areas represent a decreasing response in near infrared (linked to newly exposed areas, construction sites and new impervious surfaces), red areas represent increasing near infrared response (linked to phenological conditions of vegetation, going to an April scene to an August one), white areas represent increased response in all the visualized bands.

This approach allow to promptly visualize in RGB channels different triplets of bands at a time, thus bringing the user to a straightforward inspection of multi-spectral change features of surface objects; beginning with this visualization of multi-date information every end-user has the possibility to decide which may be the best Change Detection Technique to retrieve a land cover change map. NDR not only permits an easy and straightforward multi-

spectral comparison and evaluation of land cover changes, but permits enhanced individualization of radiometric response change, in comparison with simple Reflectance Differencing (RD). In fact, the same amount of reflectance difference between two surface features can be due to different land cover changes depending on the reference amount of spectral response. The NDR approach takes into account this issue and outputs different values of NDR for the same RD situation, when corresponding to different changes, as illustrated in the example of Figure 2 and Table 1.

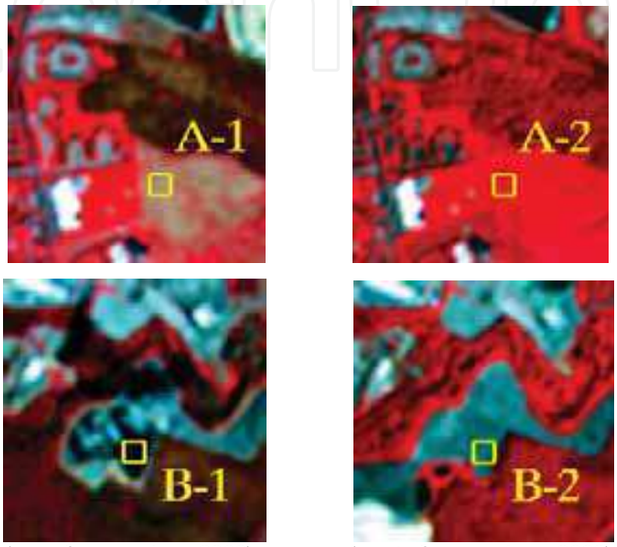

(pre-change: Apr, 2000) **(post-change: Aug, 2003)**

Fig. 2. Particular of two changed areas in an urban environment, located in Maryland, U.S.: CIR visualization (RGB=3N,2,1), ASTER scene of April 9th, 2000 (pre-change: A-1; B-1); CIR visualization (RGB=3N,2,1), ASTER scene of August 24th, 2003 (post-change: A-2; B-2): in the A area (above) a change in land cover from Bare Soil to Vegetation is highlighted in the yellow square, whereas in the B area a change in land cover from dark construction asphalt to paving concrete is highlighted in the yellow square.

Area	**Land Cover**		**NIR Reflectance Response [760-900 nm]**		**Reflectance Difference (RD)**	**Normalized Difference Reflectance (NDR)**
Fig. 2	*Pre (A-1; B-1)*	*Post (A-2; B-2)*	*pre*	*post*		
A	Bare Soil	Grass Vegetation	0.311	0.412	0.101	0.140
B	Construction Asphalt	Construction Concrete	0.103	0.207	0.104	0.335

Table 1. Normalized Reflectance Difference (NDR) results compared with common Reflectance Difference (RD) results, calculated for particular spots in Figure 2, to show the enhanced discrimination capabilities of NDR.

4. Normalized Difference Change Detyection (NDCD)

The further step to exploit the NDR approach defined and described in the previous section is its implementation in the frame of the so called Normalized Difference Change Detection (NDCD) techniques.
The NDCD technique uses the NDR defined in Equation (4.1) as input variables for deriving a land cover/land use change map through the use of one particular change detection method, thus leading to a specific implementation of the NDCD. Out of a range of techniques, such as multi-spectral transforms (e.g. Principal Components Analysis and Minimum Noise Fraction), image classification techniques (both supervised and unsupervised), image segmentation algorithms, Neural Networks or Support Vector Machines, one could be used (Lu et al., 2004).
The possible applications and purposes of this approach are manifold and diverse. In the following we will show the effectiveness of the NDCD for flood mapping. Nevertheless, this approach is a general one and might be applied not only for such mapping purposes, but also for urban growth, burnt areas mapping and other land cover change analyses.
During this work we particularly focused our research on the Minimum Noise Fraction (MNF) (Green et al., 1988; Gianinetto & Villa, 2007) implementation of the normalized difference change detection technique (NDCD-MNF), where the MNF transform is applied to the NDR data to obtain the final change detection map, for the case study analysis of the flood event due to Hurricane Katrina aftermath over the city of New Orleans, in Louisiana, U.S.. The case study and its results will be presented in the next section.
In order to give a demonstration of how the NDR and NDCD approaches work, in the following paragraphs a couple of implemented examples are show, covering a flood hazard mapping case for the monsoonal flood occurred in autumn 2000 and an urban sprawl assessment case for the suburban areas of Washington, U.S..

4.1 Flood Hazard, an Example

a) **b)** **c)**

Fig. 3. Change Detection for an monsoon flood event, which took place in the Haor region, North-East of Bangladesh: band composition visualization (RGB=7,5,3), ETM+ scene of February 28th, 2000 (a); band composition visualization (RGB=7,5,3), ETM+ scene of October 25th, 2000 (b); Change map derived with Max. Likelihood classification of NDR values.

The first example deal with a change detection application for post-flood analysis, a topic already taken into consideration by previous works of the authors (Gianinetto & Villa, 2006). The inundation event is a monsoon flooding which drawn the North of Bangladesh and North-eastern part of India in autumn 2000. A pair of Landsat ETM+ scenes covering the Haor region in north-eastern Bangladesh (the pre-event image of February 28th was normalized using post-event image of October 25th as reference) was processed and radiometrically normalized with Pseudo Invariant features (PIFs) selection and linear regression, to produce NDR values as using equation 1.
In order to map surface features changes the couple of images was inspected and regions of change were chosen as ground truth for producing a Maximum Likelihood classification and therefore a map of changed areas, shown in Figure 3. This way, not only the area covered by flooding water could be identified, but also the different vegetation phenological features due to seasonal variations was mapped (Rogan et al., 2002).

4.2 Urban Area, an Example

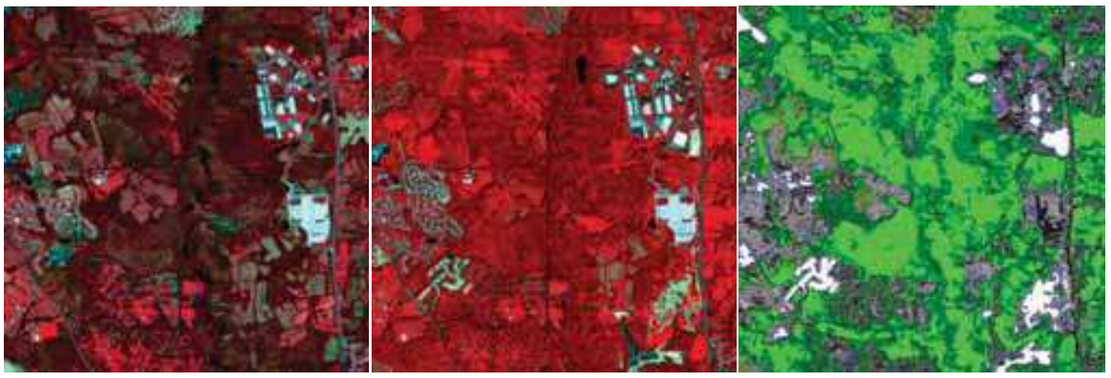

a) **b)** **c)**

Fig. 4. Change Detection for an urban scenario, located in Maryland, U.S., particular of an area of residential and commercial growth in 2000-2003 period: CIR visualization (RGB=3N,2,1), ASTER scene of April 9th, 2000 (a); CIR visualization (RGB=3N,2,1), ASTER scene of August 24th, 2003 (b); Change map derived with ISODATA classification of NDR values. Gray tones represent not changed features, green hues represent increasing vegetation vigour, bright areas represent changed surface cover: mainly newly exposed areas, construction sites and new impervious surfaces.

Another example focuses on a change detection analysis of an urbanized area for urban sprawl and its impact on environment description (Chou et al., 2005). The area covered by Terra ASTER satellite data (VIS, NIR and SWIR subset bands) is located in Maryland, U.S., in the outskirts of Washington, around 15 kilometres East of the capital's centre: the pre-change image dates back to April 9th, 2000 and was radiometrically normalized using post-change image of August 24th, 2003 as reference, using a linear regression model and PIFs.
After pre-processing and radiometric normalization, the dataset was converted to NDR values, using equation 1, and an unsupervised approach was chosen to classify changes occurred between the two dates (Bruzzone & Prieto, 2000). ISODATA classification was then performed over NDR bands and post classification labelling was utilized to assign to

retrieved classes a land cover change significance. The results are displayed in Figure 4 for a small area of detail and class colour code illustrated in caption.
The two examples presented exploit supervised or unsupervised classification of NDR values to produce change maps of a flood event (see Figure 3) or an urban growth situation (see Figure 4); the case studies tests showed a good performance in change areas delineation and identification, as a visual inspection of resulting maps witnesses. It should be pointed out that those example are only representative of a first assessment of NDR approach as an aid to Change Detection; in fact, a thoroughly assessment of the NDCD approach capabilities , together with a comparison with other Change Detection techniques results, will be done in the next section over the complete case study covering Hurricane Katrina struck New Orleans city.

5. Application Study – Flood damage assessment with NDCD

5.1 Introductive section

Recent years have seen a tremendous increase in economic and human losses from weather hazards all over the world. Major global climatic alterations are projected to occur during the 21st century and there is great concern about expected negative economic and social consequences resulting from such changes (United Nations, 2007).
Hurricane Katrina was the costliest and one of the deadliest hurricanes in the history of the USA. It was the sixth-strongest Atlantic hurricane ever recorded and the third-strongest land falling U.S. hurricane on record. At its highest intensity, Katrina was a category 5 storm on the Saffir-Simpson scale (Simpson, 1974) with wind speeds of 280 km/h.
The storm made initial landfall at Plaquemines Parish in south-eastern Louisiana on the morning of August 29 2005, and the cities of New Orleans (Louisiana), Mobile (Alabama) and Gulfport (Mississippi) bore the brunt of Katrina's force as it moved inland.
Thanks to the increasing number and observation capabilities of operational remote sensing satellites, remote sensing technology is becoming more and more used for natural hazards monitoring and management, with the great advantage of providing a synoptic vision over a wide area in a short time and in a very cost effective manner (Wang et al., 2002; Brivio et al., 2002; Sanyal & Lu, 2004; Villa & Gianinetto, 2006). In particular, remotely sensed data collected both by radar and optical satellites have been largely used for flood extent evaluation during the last 20 years and now the processing techniques are mature for an operational use (Imhoff et al., 1987; Hess et al., 1995; Frazier et al., 2003; Wang, 2004; Villa & Gianinetto, 2006; Gianinetto & Villa, 2007).
This case study exploits a new method for change detection based on the normalized difference change detection technique (NDCD). The NDCD is a technique which, given an image pair, performs calculations on radiometric normalized reflectance data through the definition of the normalized difference reflectance (NDR) and produces a standardized difference of the reflectance values.
The NDCD was used to detect the damages to the urban area of the city of New Orleans (Louisiana, USA) resulting from the passage of hurricane Katrina. Flood maps were both obtained from the image processing of SPOT-4/HRVIR and Landsat-5/TM imagery, with a suitable spatial resolution for supporting political institutions with a rapid response, effective and prompt decision maker tool.

The maps' accuracy were verified with respect to the inundation maps produced at the Dartmouth Flood Observatory, Dartmouth College (USA). A comparison was also performed between the results of the NDCD technique and that of other standard change detection methods as NIR normalized difference and spectral-temporal minimum noise fraction technique (ST-MNF).

5.2 Dataset

Remotely Sensed Dataset

The flooding caused by Hurricane Katrina over the city of New Orleans (29° 57' 33" latitude north, 90° 03' 36" longitude west) was studied using SPOT-4/HRVIR images supplied by SpotImage and the Centre National d'Etudes Spatiales (CNES) under the Optimising Access to Spot Infrastructure for Science (OASIS) Programme and Landsat-5/TM images made available from the United States Geological Survey's Earth Resources Observation and Science (USGS EROS) through the Hurricane Katrina disaster response project.

The SPOT-4/HRVIR data set was composed of:

- One 20-meters SPOT-4/HRVIR image collected on January 17, 2005 (scene ID 4 601-290 05-01-17 17:03:19 2 I) with orientation angle of 11.5 degree and incidence angle of 19.9 degree left and geocoded in UTM-WGS84 F16N projection. This image was used as pre flood image;
- One 20-meters SPOT-4/HRVIR image collected on September 19, 2005 (Scene ID 4 601-290 05-09-19 16:50:34 1 I) with orientation angle 10.0 degree and incidence angle 0.3 degree right and geocoded in UTM-WGS84 F16N projection. This image was used as post flood image.

The Landsat-5/TM data set was composed of:

- One 30-meters Landsat-5/TM image collected on June 19, 2005 (scene ID 5022039000517010), WRS-2 path 022 row 039, used as pre flood image;
- One 30-meters Landsat-5/TM image collected on September 7, 2005 (scene ID 5022039000525010), WRS-2 path 022 row 039, used as post flood image.

Additional Dataset

For the urban analysis some additional vector maps were used. The 30-meters National Land Cover Database Imperviousness Layer (NLCDIL) raster file representing urbanized and infrastructural features (impervious areas) of the city and surroundings of New Orleans (Yang et al., 2003), made available by USGS through its website (U.S. Geological Survey, 2006) was used for deriving separate mapping for the urban areas only and for the non-urban areas only.

5.3 Methodological Approach

Pre-processing

As typical in change detection applications and as envisaged in the earlier part of this work, about pre-processing of data for change analysis, geocoding and atmospheric correction are always needed. For this purposes the satellite data were first georeferenced in the UTM-WGS84 projection, using reference data. Original at-sensor radiance data were atmospherically corrected using a low resolution Radiative Transfer Code, combined with aerosol retrieval based on band reflectance ratios and with adjacency correction of path radiance (Berk et al., 1999; Vermote et al., 1997).

A further step is the radiometric normalization of multispectral data, carried out using a parabolic parametric model:

$$R_j^{norm} = a_j (R_j^{raw})^{b_j} \tag{2}$$

where:

R^{norm} = normalized reflectance
R^{raw} = input reflectance of the slave image
a = multiplicative coefficient of the parametric model
b = exponential coefficient of the parametric model
j = spectral band number

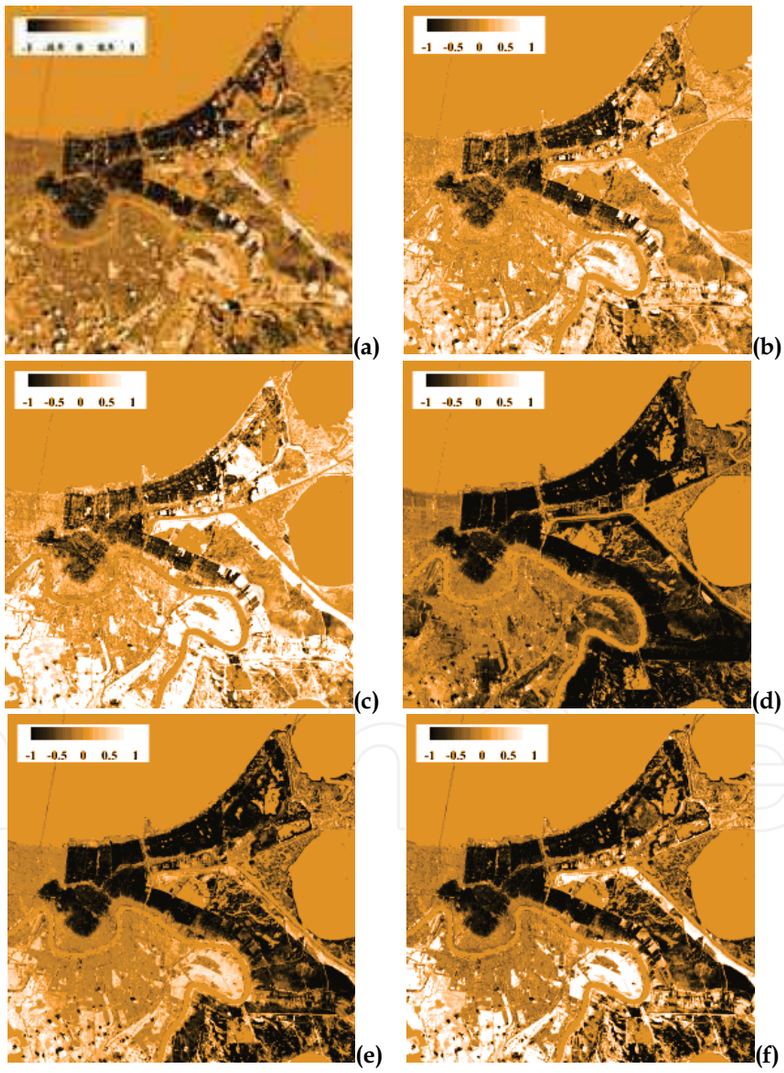

Fig. 6. Example of normalized difference reflectance (NDR) calculated for the Landsat-5/TM dataset. (a) Spectral band nr.1; (b) Spectral band nr.2; (c) Spectral band nr.3; (d) Spectral band nr.4; (e) Spectral band nr.5; (f) Spectral band nr.7.

The radiometric normalization of reflectance data was performed using a parametric parabolic model based on equation 2 through standard linearized least square matching based on a parametric model and an iteration approach to solution of the linearized basic observation equation. The transformation coefficients were computed using standard linearized least squares matching, through an iteration approach to solution of the linearized basic observation equation.
Radiometrically normalized data were used for calculating NDR values for both Landsat-5/TM and SPOT-4/HRVIR data, using the approach described in the previous sections and calculated with equation (4.1). The NDR values were finally used as inputs for Minimum Noise Fraction (MNF) transform, thus structuring the implementation of the NDCD-MNF technique for change mapping and flooded area delineation.

Mapping Hurricane Katrina's aftermaths in New Orleans
The widespread destruction in New Orleans was mapped using the NDCD-MNF technique. The SPOT-4/HRVIR and Landsat-5/TM images were first radiometrically normalized using the parametric model of equation (2.2) and the NDR were computed using equation (4.1). Following, to the multi-spectral NDR values it was applied the MNF transform, generating the normalized difference reflectance-Minimum Noise Fraction (NDR-MNF) components.
From all the NDR-MNF components generated, only the first and the second were retained, being the most representative of a good identification of water related land cover. By visual interpretation of the post flood images, the final selection of the best representative NDR-MNF component (component nr.1 or component nr.2) was carried out and the final mapping was realized by using an adaptive threshold. Figure 7 shows the NDR-MNF component nr.2 for SPOT-4/HRVIR (Figure 7a) and Landsat-5/TM (Figure 7b), subsequently used for the mapping.

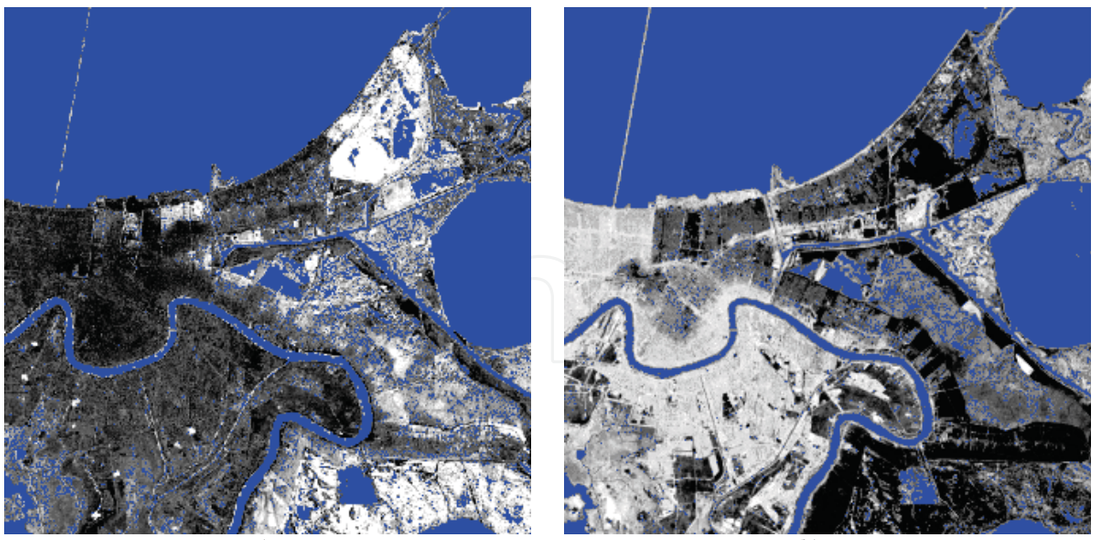

a) b)

Fig. 7. Normalized Difference Reflectance-Minimum Noise Fraction (NDR-MNF) component nr.2 used for the mapping. (left) SPOT-4/HRVIR; (right) Landsat-5/TM.

The criteria used for the threshold selection was based on the detection of the maximum separability interval between flooded and non-flooded areas. For the SPOT-4/HRVIR and Landsat-5/TM image data some samples of the selected NDCD-MNF component were independently extracted, belonging to the urban and non-urban land cover classes, both for the flooded and non-flooded areas.
For the Landsat-5/TM data set, 900 pixels were selected for the urbanized areas (400 pixels in flooded area and 500 in non-flooded area), covering nearly 0.2% of the total urbanized areas, while 1,200 pixels were selected for the non-urbanized areas (700 pixels in flooded area and 500 in non-flooded area), covering nearly 0.2% of the total non-urbanized areas.
For the SPOT-4/HRVIR data set, 1,500 pixels were selected for the urbanized areas (600 pixels in flooded area and 900 in non-flooded area), covering nearly 0.15% of the total urbanized areas, while 2,000 pixels were selected for the non-urbanized areas (1,200 pixels in flooded area and 800 in non-flooded area), covering nearly 0.15% of the total non-urbanized areas.
For all these samples, the first and second-order statistics were computed and the maximum separability interval between the flooded and non-flooded areas was identified by testing different threshold values belonging to the interval; finally the global flood maps were produced.
Next, using the USGS's NLCDIL as supplementary input data, three other products were generated from the SPOT-4/HRVIR and the Landsat-5/TM data sets: i) a flood map for the 'urban areas only'; ii) a flood map for the 'non-urban areas only'; and iii) a 'fused' flood map:

i) The flood map for the **urban areas** only was built using the non-impervious surface layer of the NLCDIL as mask for excluding from the processing all the image pixels collected on non-urban areas;
ii) The flood map for the **non-urban areas** only was built using the impervious surface layer of the NLCDIL as mask for excluding from the processing all the image pixels collected on urban areas;
iii) The **fused** flood map was built fusing together the results previously obtained for the urban areas only and the non-urban areas only. This processing returned a product comparable to the global flood map above described, but it has proven more accurate.

To boost the spatial coherency and homogeneity of the final mapping, all the flood maps were refined with classical segmentation and clumping techniques.

5.4 Performance Evaluation and Comparison to other techniques

The accuracies of all the maps produced with the NDCD-MNF technique were verified using as ground truth the flood extension map of the city of New Orleans (Figure 8) produced at the Dartmouth Flood Observatory (Dartmouth College, USA) and provided by courtesy of Prof. G.R. Brakenridge and Dr. E. Anderson (Dartmouth College, USA).
The potentialities and performances of the NDCD technique for flood mapping were also compared to following standard change detection methods characterized by different complexity:

- Change detection based on the near-infrared normalized difference (Hayes and Sader, 2001);
- Spectral-Temporal Minimum Noise Fraction (ST-MNF) technique previously developed by authors for flood mapping (Gianinetto & Villa, 2007).

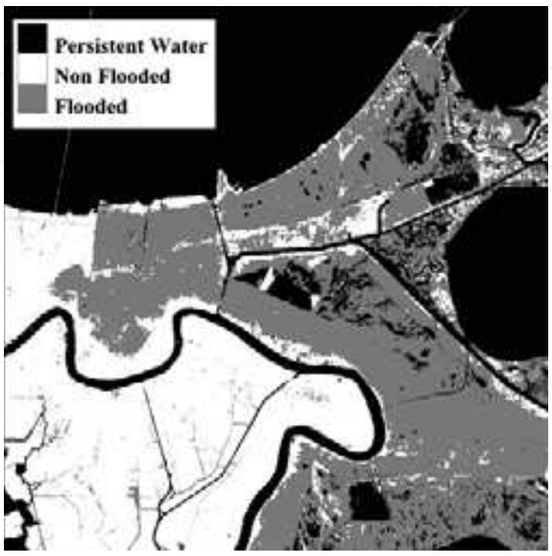

Fig. 8. 20-meters resolution raster image derived from the vector flood extension map produced at the Dartmouth Flood Observatory (Dartmouth College, USA).

NIR normalized difference change detection

The simplest change detection technique used to compare the results obtained using the NDCD-MNF was based on the NIR normalized difference (Hayes and Sader, 2001). Using only the infrared band (TM4 for Landsat-5/TM and XS3 for SPOT-4/HRVIR) it was produced a flood map by thresholding the normalized difference between the post-flood and pre-flood images.

Similarly to the processing carried on with the NDCD-MNF, also using the NIR normalized difference it were separately calculated: i) a flood map for the urban areas only, ii) a the flood map for the non-urban areas only, and iii) a global flood map, both for the SPOT-4/HRVIR and the Landsat-5/TM data set.

Spectral-Temporal Minimum Noise Fraction technique

Another term of comparison for the NDCD-MNF method was the ST-MNF technique previously developed by the authors (Gianinetto & Villa, 2006; Gianinetto & Villa, 2007).

In this case only the global flood maps were generated for both the Landsat-5/TM and SPOT-4/HRVIR data set by processing together both the impervious and non-impervious land cover features. Starting from the pre-processed normalized images, a synthetic n-band file (with n=8 for SPOT-4/HRVIR and n=12 for Landsat-5/TM) was created including first the reflective bands of the pre flood scene followed by the homologous bands of the post flood scene, stacked together. To this Spectral-Temporal merging it was applied the MNF transform and a thresholding to derive the flood extension map, whereas a complete description of the ST-MNF technique can be found in (Gianinetto & Villa, 2007).

5.5 Results and Discussion

Sampling for accuracy assessment
The testing samples used for the accuracy assessment of the flood maps were selected following a stratified random sampling approach over the datasets. In detail, accuracy test samples were collected as:

a) For the SPOT-4/HRVIR data set:
   i) 9,921 samples on reference ground truth data (1.0% of the total) for the urbanized areas: 4,017 samples in flooded areas (40.5%) and 5,904 samples in non-flooded areas (59.5%).
   ii) 13,568 samples on reference ground truth data (1.0% of the total) for the non-urbanized areas: 8,158 samples in flooded areas (60.1%) and 5,410 samples in non-flooded (39.9%).
   iii) 11,812 samples on reference ground truth data (0.5% of the total) for the whole area, 6,449 samples in flooded areas (54.6%) and 5,363 samples in non-flooded areas (45.4%).
b) For the Landsat-5/TM data set:
   i) 8,726 samples on reference ground truth data (2.0% of the total) for the urbanized areas: 3,401 samples in flooded (39.0%) and 5,325 samples in non-flooded areas (61.0%).
   ii) 11,608 samples on reference ground truth data (2.0% of the total) for the non-urbanized areas: 6,580 samples in flooded areas (56.7%) and 5,028 samples in non-flooded areas (43.3%).
   iii) 15,596 samples on reference ground truth data (1.5% of the total) for the whole area: 7,878 samples in flooded areas (50.5%) and 7,718 samples in non-flooded areas (49.5%).

Mapping accuracy using the NDCD-MNF technique
Flood maps for the 'urban areas only' and for the 'non-urban areas only', along with a 'fused' flood map were obtained by thresholding the NDR-MNF component nr.1.
Regarding the flood mapping in the urban areas only, the data processing performed on the Landsat-5/TM imagery led to higher accuracy than those performed on the SPOT-4/HRVIR imagery (Table 2, Figure 9). For the former it was obtained a best Overall Accuracy (OA) of 92.05% and a kappa coefficient (K) of 0.83, while for the latter the results gave an OA of 86.37% and a K of 0.72.

The threshold selection was not a critical issue for the Landsat-5/TM data, while for the SPOT-4/HRVIR data, approaching to the upper (positive) limit of the separability interval the accuracy became worse (OA=72.30, K=0.48). In any case, regardless the threshold value selection, the mapping based on the Landsat-5/TM images was always superior to those based on the SPOT-4/HRVIR images.
On the contrary, with respect to the flood mapping in the 'non-urban areas only', the data processing performed on the Landsat-5/TM imagery led to lower accuracy than those performed on the SPOT-4/HRVIR imagery (Table 3, Figure 10). For the former it was obtained a best OA of 75.70% and a K of 0.49, while for the latter the results gave an OA of 86.31% and a K of 0.71.

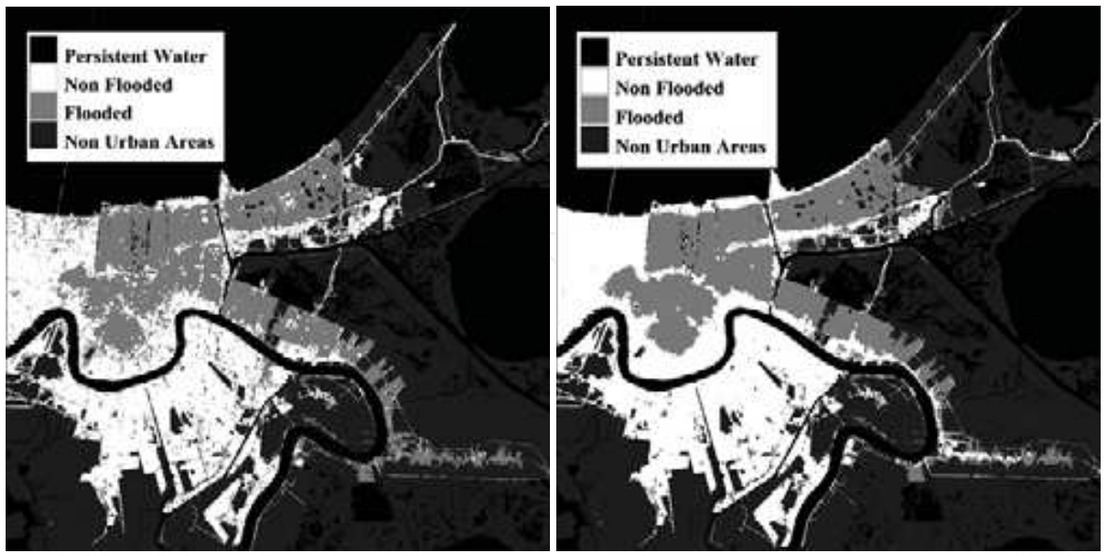

Fig. 9. New Orleans (Louisiana). Flood mapping in the urban areas only using the NDCD-MNF technique. (left) Derived from SPOT-4/HRVIR data; (right) Derived from Landsat-5/TM data.

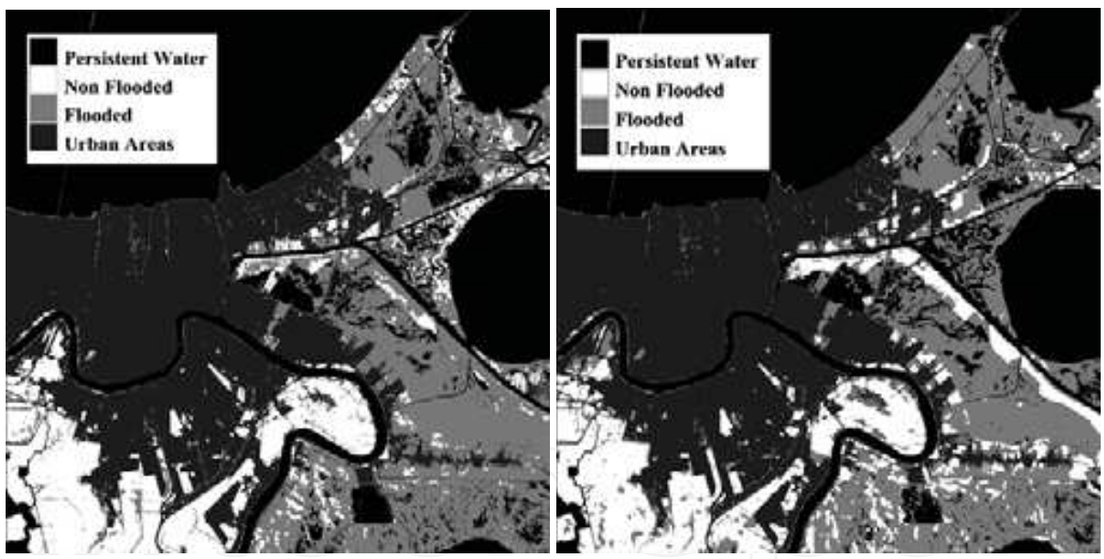

Fig. 10. New Orleans (Louisiana). Flood mapping in the non-urban areas only using the NDCD -MNF technique. (left) Derived from SPOT-4/HRVIR data; (right) Derived from Landsat-5/TM data.

The threshold selection was not a critical issue both for the Landsat-5/TM and for the SPOT-4/HRVIR data. In any case, regardless of the threshold value selection, this time the mapping based on the SPOT-4/HRVIR images was always superior to those based on the Landsat-5/TM images.

	Threshold value	Overall Accuracy * (%)	K coefficient
SPOT-4 /HRVIR data set	-2.0	85.72	0.70
	-1.5	86.37	0.72
	-1.0	84.96	0.69
	0.0	72.30	0.48
Landsat-5/TM data set	-1.0	89.69	0.79
	0.0	90.52	0.80
	1.0	92.05	0.83
	2.0	91.16	0.81

* Values in bold indicate the best accuracy.

Table 2. Flood mapping in the 'urban areas only' using the NDCD-MNF technique. Threshold selection and mapping accuracy.

	Threshold value	Overall Accuracy * (%)	K coefficient
SPOT-4 /HRVIR data set	0.0	85.56	0.69
	0.5	86.31	0.71
	1.0	86.17	0.70
	2.0	84.0	0.65
Landsat-5/TM data set	-1.5	75.59	0.49
	-1.0	75.70	0.49
	-0.5	75.11	0.48
	0.0	74.34	0.47

* Values in bold indicate the best accuracy.

Table 3. Flood mapping in the 'non-urban areas only' using the NDCD-MNF technique. Threshold selection and mapping accuracy.

The reason of the poor mapping in non-urban areas using the Landsat-5/TM dataset may be found in the closeness of the post-flood image (September 7, 2005) to Katrina landfall (August 29, 2005). In the Landsat-5/TM post-flood image many wet areas (rain-washed), mainly located in non urbanized areas (impervious surfaces), were incorrectly detected as flooded. This phenomena was not observed in the SPOT-4/HRVIR post-flood image because of the longer time elapsed from the passage of Katrina (September 19, 2005).

A global 'fused' flood map was obtained by fusing together of the urbanized and non-urbanized flood maps separately computed with the NDCD-MNF technique (Figure 11). In this case, the comparison of global results from the Landsat-5/TM (OA=84.03% and K=0.68) and SPOT-4/HRVIR (OA=86.36% and K=0.73) data processing are similar, with a little advantage for the SPOT-based mapping. This result is justified by the non homogeneous accuracy of the Landsat-based mapping in urban and non urban areas, as previous described (Table 2 and Table 3).
A simpler and less computational expensive global flood map was derived by processing together both the urban and non-urban areas in a single step (Figure 12). Differently to the previous cases, the NDR-MNF component nr.2 was used this time for the thresholding of both the dataset.

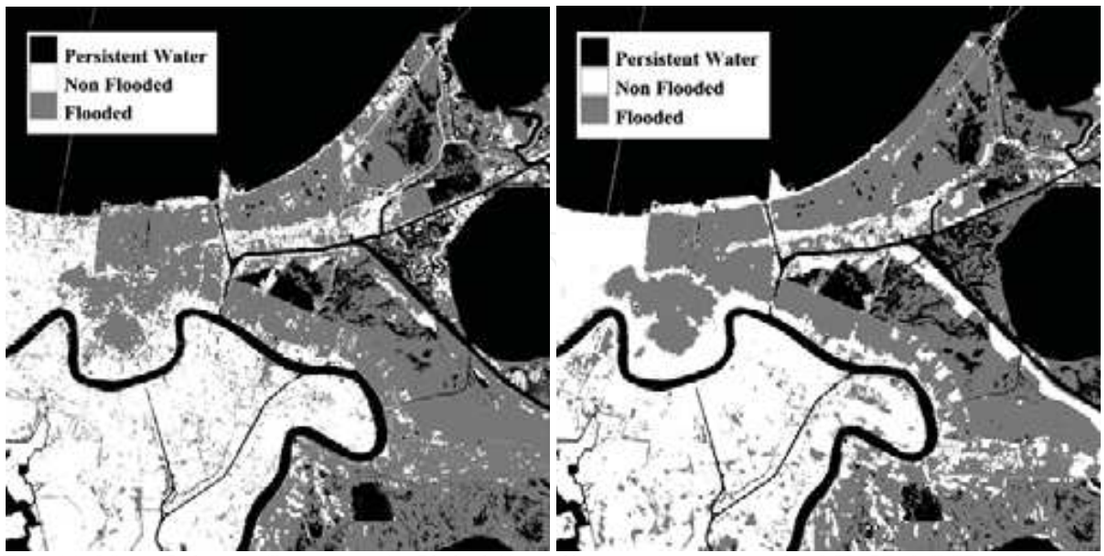

Fig. 11. New Orleans (Louisiana). Global 'fused' mapping using the NDCD-MNF technique. (left) Derived from SPOT-4/HRVIR data; (right) Derived from Landsat-5/TM data.

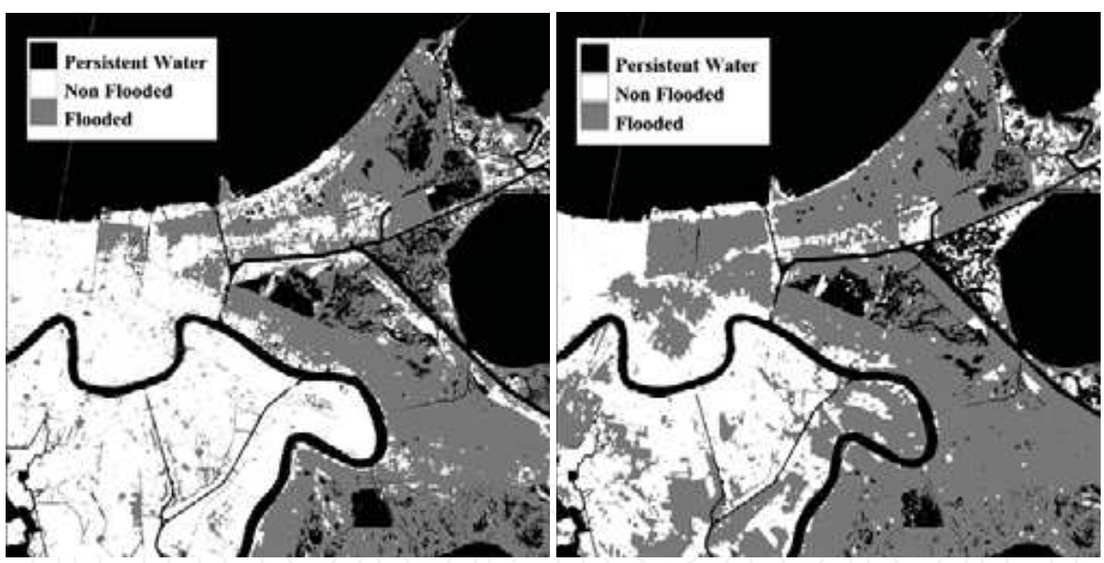

Fig. 12. New Orleans (Louisiana). Global flood map using the NDCD-MNF technique. (left) Derived from SPOT-4/HRVIR data; (right) Derived from Landsat-5/TM data.

Again the Landsat-5/TM data processing led to lower accuracy (OA=77.32% and K=0.54) than the SPOT-4/HRVIR data processing (OA=83.20% and K=0.67), when compared to ground truth data, mainly due to its lower accuracy in the non-urban areas (Table 4).

	Threshold value	Overall Accuracy * (%)	K coefficient
SPOT-4 /HRVIR data set	-2.0	66.11	0.28
	-1.0	82.02	0.63
	-0.5	83.20	0.67
	0.0	82.24	0.65
	1.0	75.92	0.53
Landsat-5/TM data set	0.0	76.60	0.53
	1.0	77.32	0.54
	2.0	75.81	0.51
	3.0	72.50	0.45

* Values in bold indicate the best accuracy.

Table 4. Global flood mapping using the NDCD-MNF technique when processing together both the impervious and non-impervious surfaces. Threshold selection and mapping accuracy.

This time, for the SPOT-4/HRVIR dataset both the NDR-MNF component selection and the threshold selection are critical and the accuracy largely depends upon their correct identification. Regarding the NDR-MNF component selection, when using component 1 instead of component 2, as in previous cases, for the Landsat-5/TM data processing we had a little decrease in the mapping accuracy (from 77.32% to 75.50% for the OA), while for the SPOT-4/HRVIR data processing a greater decrease in the mapping accuracy was observed (from 83.20% to 67.74% for the OA).
The foremost advantage of this single step global mapping is that no urban mask is required, so no a priori information is needed to separate impervious from non impervious surfaces. On the other hand, the mapping accuracy is always worse when compared to the global 'fused' map obtained by fusing together of the urbanized and non-urbanized flood maps separately computed (Figure 11). For the SPOT-4/HRVIR data it was observed a decrease in the OA from 86.36% to 83.20% and a decrease in the K from 0.73 to 0.67, while for the Landsat-5/TM data it was observed a larger decrease both in the OA from 84.36% to 77.32% and in the K from 0.68 to 0.54 (Table 4).

Comparing the mapping accuracy of the NDCD-MNF to the NIR-normalized difference change detection

Using the NIR-normalized difference change detection it was generated a global flood map by processing together both the urban and the non-urban areas (Figure 13) and a global 'fused' flood map by processing separately the urban and the non-urban areas (Figure 14).
This technique seems to be insensitive to both the data set used (SPOT-4/HRVIR or Landsat-5/TM) and to the data processing adopted (global or 'fused' map), leading to an OA between 81.66% and 82.75% and a K between 0.63 and 0.66. Table 5 shows a summary of results.
When comparing the NDCD-MNF to the NIR-normalized difference change detection it emerged the superiority of the former in all the 'fused' products (OA=86.36 and K=0.73 for the SPOT-4/HRVIR data set and OA=84.36 and K=0.68 for the Landsat-5/TM data set) and a better accuracy for the latter with respect to only the Landsat-5/TM global flood map (OA=82.03% and K=0.64).

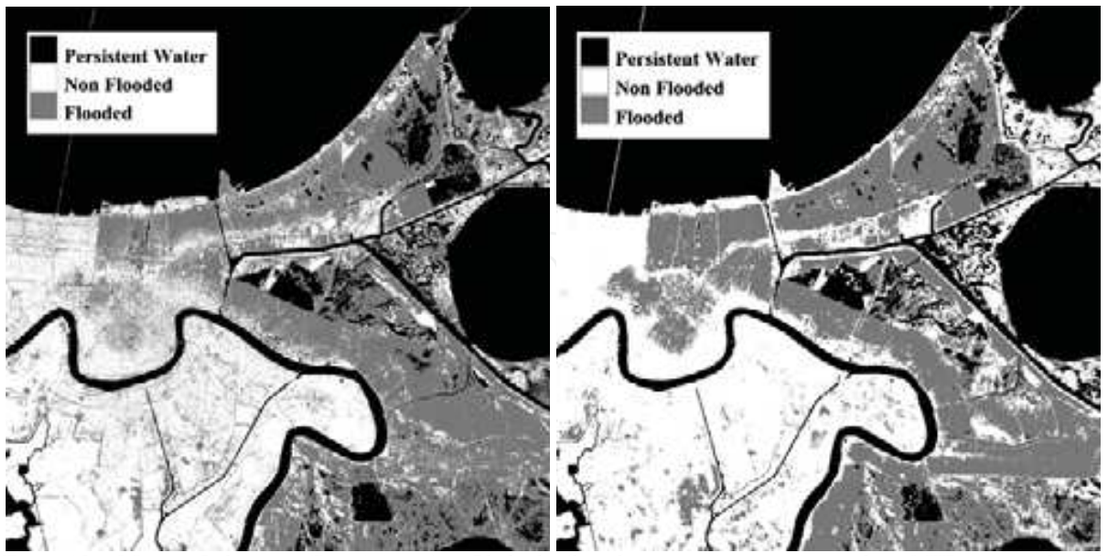

Fig. 13. New Orleans (Louisiana). Global flood mapping using the NIR-normalized difference technique. (left) Derived from SPOT-4/HRVIR; (right) Derived from Landsat-5/TM.

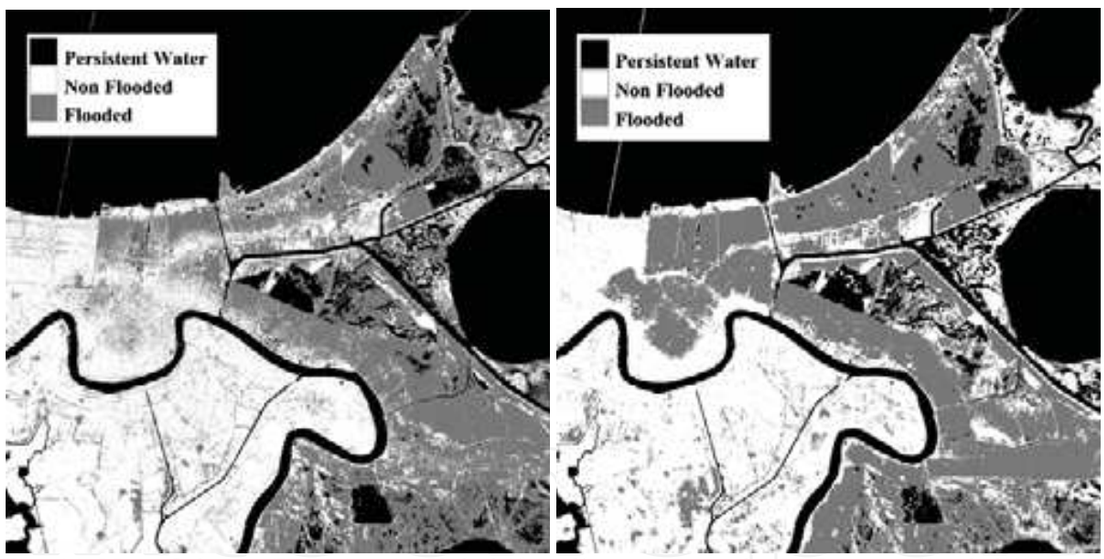

Fig. 14. New Orleans (Louisiana). Global 'fused' map using the NIR-normalized difference technique. (left) Derived from SPOT-4/HRVIR; (right) Derived from Landsat-5/TM.

	Threshold Value	Overall Accuracy * (%)	K coefficient
SPOT-4 /HRVIR data set	-0.100	79.13	0.59
	-0.075	81.07	0.62
	-0.050	81.73	0.63
	-0.025	80.83	0.61
Landsat-5/TM data set	-0.35	79.92	0.60
	-0.30	82.03	0.64
	-0.25	81.95	0.64
	-0.20	80.16	0.60

* Values in bold indicate the best accuracy.

Table 5. Global flood mapping using the NIR-normalized difference change detection technique. Threshold selection and mapping accuracy.

Comparing the mapping accuracy of the NDCD-MNF to the Spectral-Temporal Minimum Noise Fraction technique

Using the ST-MNF technique it was generated a global flood map by processing together both the urban and the non-urban areas on the basis of the MNF component nr. 1 for both the data set (Figure 15).

The threshold selection here revealed to be not a critical issue for the mapping accuracy. By using the ST-MNF technique, the Landsat-5/TM data processing led to higher accuracy (OA=90.17% and K=0.80) than the SPOT-4/HRVIR data processing (OA=81.87% and K=0.63) when compared to ground truth data. Table 6 shows a summary of results.

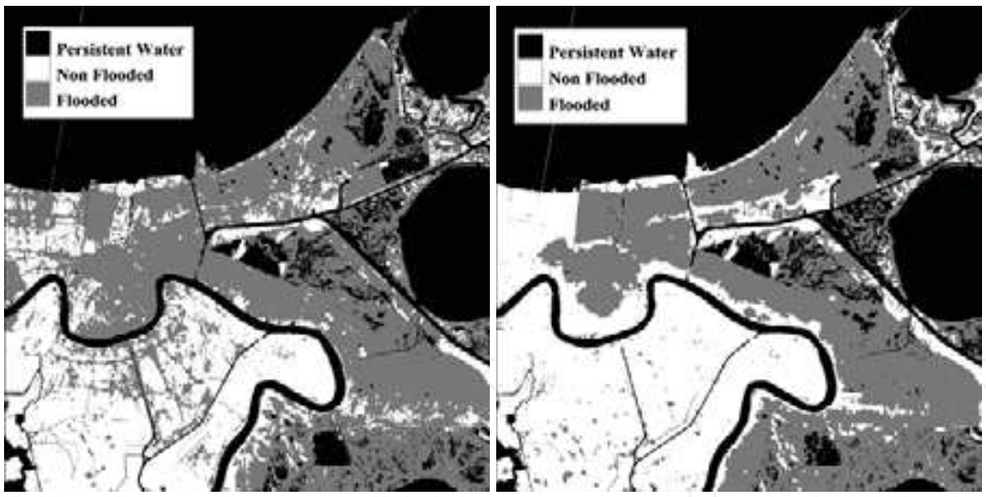

Fig. 15. New Orleans (Louisiana). Global damages mapping using the ST-MNF technique. (left) Derived from SPOT-4/HRVIR data; (right) Derived from Landsat-5/TM data.

A comparison between the NDCD-MNF and the ST-MNF shows that the former always performed better on the SPOT-4/HRVIR data set, regardless the data processing used for the global mapping used (with or without urban areas masking). While with respect to the Landsat-5/TM data set, results are more difficult to analyse. Looking at the OA only it seems that the ST-MNF led to higher accuracy (OA=90.17 for ST-MNF and OA=84.36 for NDCD-MNF), but the K score of the NDCD-MNF is higher for the 'fused' map (K=0.68 for

NDCD-MNF and K=0.63 for ST-MNF). So it is difficult to say which performed better with respect to the overall situation.

	Threshold value	Overall Accuracy * (%)	K coefficient
SPOT-4 /HRVIR data set	-1.0	81.76	0.63
	-0.5	81.87	0.63
	0.0	81.43	0.62
	1.0	79.33	0.58
Landsat-5/TM data set	-1.0	89.37	0.78
	0.0	89.79	0.79
	0.5	90.12	0.80
	1.0	90.17	0.80
	2.0	89.71	0.79

* Values in bold indicate the best accuracy.

Table 6. Global flood mapping using the ST-MNF technique. Threshold selection and mapping accuracy.

5.6 Summary and Coclusions

This case study tested the normalized difference change detection technique effectiveness for change mapping, also in comparison with other literature methodologies, starting from the processing of the normalized difference reflectance data.

The radiometric normalization of data influenced the accuracy of the mapping. A parametric normalization with coefficients calculated with standard linearized least squares adjustment and iterative solution was found a better solution than a standard linear normalization, and thus adopted. However, the general definition of the NDCD leaves the possibility to develop processing techniques based on different radiometric normalization schemes.

Using its MNF implementation, the NDCD technique was used for mapping and evaluating the havoc on the city of New Orleans (Louisiana, USA) wreaked by Hurricane Katrina landfall in August 2005, using both a SPOT-4/HRVIR and a Landsat-5/TM data set.

As a term of comparison for evaluating the potentialities and performances of the NDCD-MNF technique, several other standard change detection methods have been tested: from the simple NIR normalized difference to the more complex Spectral-Temporal Minimum Noise Fraction technique.

Comparing the global mapping accuracy when using the SPOT-4/HRVIR data, the NDCD-MNF technique always leaded to better results than all the others methods here taken into consideration. Moreover, results were better when processing separately the urban and the non-urban areas in the so called 'fused' product.

With regards to the Landsat-5/TM data, the NDCD-MNF technique poorly performed in the non-urban areas (probably due to the closeness of the post-flood image to Katrina landfall), thus affecting the final global mapping. However, with respect to the only urban areas, which may be of major interest in most cases, the NDCD-MNF always performed better.

Finally, regarding the threshold selection, a number of studies [Yuan et al., 1998; Chen et al., 2003] have pointed out that a major weakness of all spectral change detection approaches is that the selection of a minimum threshold to signify change is often arbitrary [Warner,

2005]. For example, a threshold value of two standard deviations above the mean is sometimes selected (Sohl, 1999). To address this problem, some studies used a noise model to select the threshold (Dwyer et al., 1996). As an alternative, other studies have developed a systematic method using training data (Chen et al., 2003). In their approach, areas of change are digitized, as well as a surrounding window of no change. These training areas are then classified into 'change' and 'no change' classes, using a small number of arbitrarily chosen thresholds spread over a wide range of possible values. Based on the accuracies of these classifications, the range of thresholds is narrowed successively to focus on the region where the accuracy is highest. In this iterative fashion, an optimal threshold is selected.

The accuracy gained through NDR approach derived changes mapping have been proven very satisfying most of the times, with Overall Accuracies percentage figures ranging from 80% to over 90% of correctness, that is to say error percentage in change mapping around 10% which is to be considered as a really good result for analysis performed and based only on remote sensing satellite data.

Nevertheless, more testing and a more fine tuning of the processing chain can be implemented and done in the future, including not yet explored land cover change application fields, and the good results achieved until now are a great encouragement to continue on the path already traced with the works described in this chapter.

6. References

Berk, A., Anderson, G. P., Bernstein, L. S., Acharya, P. K., Dothe, H., Matthew, M. W, Adler-Golden, S. M., Chetwynd, J. H., Richtsmeier, S. C., Pukall, B., Allred, C. L., Jeong, L. S., and Hoke, M. L., (1999); MODTRAN4 Radiative Transfer Modeling for Atmospheric Correction, *SPIE Proceedings, Optical Spectroscopic Techniques and Instrumentation for Atmospheric and Space Research III*, vol. 3756, pp.348-353

Brivio, P. A., Colombo, R., Maggi, M., and Tomasoni, R., (2002); Integration of remote sensing data and GIS for accurate mapping of flooded areas, *International Journal of Remote Sensing*, 23(3), pp. 429-441.

Bruzzone, L., and Fernàndez Prieto, D., (2000); Automatic Analysis of the Difference Image for Unsupervised Change Detection, *IEEE Transactions on Geoscience and Remote Sensing*, vol. 38, no. 3, pp.1171-1182.

Chen, J., Gong, P. and Shi, P., (2003); Land-use/land-cover change detection using improved change-vector analysis, *Photogrammetric Engineering and Remote Sensing*, 69 , pp. 369-379.

Chou, T. Y., Lei, T. C., Wan, S., and Yang, L. S., (2005); Spatial knowledge databases as applied to the detection of changes in urban land use, *International Journal of Remote Sensing*, vol. 26, no. 14, pp. 3047-3068.

Coppin, P., and Bauer, M.E., (1994); Digital Processing of Multitemporal Landsat TM Imagery to Optimize Extraction of Forest Cover Change Features, *IEEE Transactions on Geoscience and Remote Sensing*, 32(4), pp. 918-927.

Coppin, P., Nackaerts, K., Queen, L., and Brewer, K., (2001); Operational Monitoring of Green Biomass Change for Forest Management, *Photogrammetric Engineering & Remote Sensing*, 67(5), pp. 603-611.

Coppin, P., Jonckheere, I., Nackaerts, K., Muys, B., and Lambin, E., (2004); Digital change detection methods in ecosystem monitoring: a review, *International Journal of Remote Sensing*, 25(9), pp. 1565-1596.

Dwyer, J.L., Sayler, K.L., and Zylstra, G.J., (1996); Landsat pathfinder data sets for landscape change analysis. *Proceedings of the 1996 IEEE International Geoscience and Remote Sensing Symposium, IGARSS 1996*, Lincoln, Nebraska, pp. 547-550.

Frazier, P., Page, K., Louis, J., Briggs, S., and Robertson, A. I., (2003); Relating wetland inundation to river flow using Landsat TM data, *International Journal of Remote Sensing*, 24(19), pp. 3755-3770.

Gianinetto, M., and Villa, P., (2006); Monsoon Flooding Response: a Multi-scale Approach to Water-extent Change Detection, *The International Archive of the Photogrammetry, Remote Sensing and Spatial Information Sciences, XXXVI(7)*, Enschede, the Netherlands, pp. 128-133.

Gianinetto, M., and Villa, P., (2007); Rapid Response Flood Assessment Using Minimun Noise Fraction And Composed Spline Interpolation, *IEEE Transactions on Geoscience and Remote*, 45(10), pp. 3204-3211.

Green, A.A., Berman, M., Switzer, P., and Craig, M.D., (1988); A transformation for ordering multispectral data in terms of image quality with implications for noise removal, *IEEE Transactions on Geoscience and Remote Sensing*, 26(1), pp. 65-74.

Hayes, D.J., and Sader, S.A., (2001); Comparison of Change-Detection Techniques for Monitoring Tropical Forest Clearing and Vegetation Regrowth in a Time Series, *Photogrammetric Engineering and Remote Sensing*, 67(9), pp. 1067-1075.

Hess, L.L., Melack, J.M., Filoso, S., and Wang, Y., (1995); Realtime mapping of inundation on the Amazon floodplain with the SIR-C/X-SAR synthetic aperture radar, *IEEE Transactions on Geoscience and Remote Sensing*, 33, pp. 896-904.

Imhoff, M. L., Vermillon, C., Story, M. H., Choudhury, A. M., and Gafoor, A., (1987); Monsoon flood boundary delineation and damage assessment using spaceborne imaging radar and Landsat data, *Photogrammetric Engineering and Remote Sensing*, 4, pp. 405-413.

Lu, D., Mausel, P., Brondizio, E., and Moran, E., (2004); Change detection techniques, *International Journal of Remote Sensing*, 25, pp. 2365-2407.

Rogan, J., Franklin, J., Roberts, D. A., (2002); A comparison of methods for monitoring multitemporal vegetation change using Thematic Mapper imagery, *Remote Sensing of Environmen*t, vol. 80, pp. 143-156.

Sanyal, J., and Lu X., X., (2004); Application of the Remote Sensing in Flood Management with Special Reference to Monsoon Asia: a Review, *Natural Hazards*, 33, pp. 283-301.

Simpson, R.H., (1974); The hurricane disaster-potential scale, *Weatherwise*, 27, pp. 169.

Singh, A., (1989); Digital change detection techniques using remotely-sensed data, *International Journal of Remote Sensing*, 10(6), pp. 989-1003.

Sohl, T.L., (1999); Change analysis in the United Arab Emirates: an investigation of techniques, *Photogrammetric Engineering and Remote Sensing*, 65, pp. 475-484.

U.S. Geological Survey, (2001); *National Land Cover Database 2001 (NLCD 2001)*, digital resource available online at: www.mrlc.gov/mrlc2k_nlcd.asp.

United Nations, (2007); *Evidence is now 'unequivocal' that humans are causing global warming*, UN report.

Vermote E., Tanré D., Deuzé J. L., Herman M., Morcrette J. J., (1997); Second Simulation of the Satellite Signal in the Solar Spectrum, 6S: An Overview, *IEEE Transactions on Geoscience and Remote Sensing*, 35(3), pp. 675-686.

Villa, P., and Gianinetto, M., (2006); Multispectral transform and Spline Interpolation for Mapping Flood Damages, *Proceedings of the 2006 IEEE International Geoscience and Remote Sensing Symposium, IGARSS 2006*, Denver, U.S., pp. 275-279.

Villa, P., and Lechi, G., (2007); Normalized Difference Reflectance: An Approach to Quantitative Change Detection, *Proceedings of the 2007 IEEE International Geoscience and Remote Sensing Symposium, IGARSS 2007*, Barcelona, Spain, pp. 2366-2369.

Wang, Y., Colby, J.D., and Mulcahy, K.A., (2002); An efficient method for mapping flood extent in a coastal flood plain using Landsat TM and DEM data, *International Journal of Remote Sensing*, 23(18), pp. 3681-3696.

Wang, Y., (2004); Using Landsat 7 TM data acquired days after a flood event to delineate the maximum flood extent on a coastal floodplain, *International Journal of Remote Sensing*, 25(5), pp. 959-974.

Yang, L., Huang, C., Homer, C.G., Wylie, B.K., and Coan, M.J., (2003); An approach for mapping large-area impervious surfaces: synergistic use of Landsat-7 ETM+ and high spatial resolution imagery, *Canadian Journal of Remote Sensing*, 29(2), pp. 230-240.

IntechOpen

Geoscience and Remote Sensing

Edited by Pei-Gee Peter Ho

ISBN 978-953-307-003-2
Hard cover, 598 pages
Publisher InTech
Published online 01, October, 2009
Published in print edition October, 2009

Remote Sensing is collecting and interpreting information on targets without being in physical contact with the objects. Aircraft, satellites ...etc are the major platforms for remote sensing observations. Unlike electrical, magnetic and gravity surveys that measure force fields, remote sensing technology is commonly referred to methods that employ electromagnetic energy as radio waves, light and heat as the means of detecting and measuring target characteristics. Geoscience is a study of nature world from the core of the earth, to the depths of oceans and to the outer space. This branch of study can help mitigate volcanic eruptions, floods, landslides ... etc terrible human life disaster and help develop ground water, mineral ores, fossil fuels and construction materials. Also, it studies physical, chemical reactions to understand the distribution of the nature resources. Therefore, the geoscience encompass earth, atmospheric, oceanography, pedology, petrology, mineralogy, hydrology and geology. This book covers latest and futuristic developments in remote sensing novel theory and applications by numerous scholars, researchers and experts. It is organized into 26 excellent chapters which include optical and infrared modeling, microwave scattering propagation, forests and vegetation, soils, ocean temperature, geographic information , object classification, data mining, image processing, passive optical sensor, multispectral and hyperspectral sensing, lidar, radiometer instruments, calibration, active microwave and SAR processing. Last but not the least, this book presented chapters that highlight frontier works in remote sensing information processing. I am very pleased to have leaders in the field to prepare and contribute their most current research and development work. Although no attempt is made to cover every topic in remote sensing and geoscience, these entire 26 remote sensing technology chapters shall give readers a good insight. All topics listed are equal important and significant.

InTech Europe
University Campus STeP Ri

InTech China
Unit 405, Office Block, Hotel Equatorial Shanghai

Slavka Krautzeka 83/A
51000 Rijeka, Croatia
Phone: +385 (51) 770 447
Fax: +385 (51) 686 166
www.intechopen.com

No.65, Yan An Road (West), Shanghai, 200040, China
中国上海市延安西路65号上海国际贵都大饭店办公楼405单元
Phone: +86-21-62489820
Fax: +86-21-62489821

IntechOpen

IntechOpen